Journal of Materials Chemistry B

ROYAL SOCIETY OF CHEMISTRY

PAPER

View Article Online
View Journal | View Issue

Cite this: J. Mater. Chem. B, 2024, 12, 3092

Mussel-inspired PDA@PEDOT nanocomposite hydrogel with excellent mechanical strength, self-adhesive, and self-healing properties for a flexible strain sensor†

Xiaoyi Li,‡[ab] Xueshan Zhao,‡[c] Ruiqi Liu,[c] Hui Wang,[d] Shuang Wang,[ab] Bing Fan,[e] Chenggong Hu*[ab] and Haibo Wang [ab]

Received 18th November 2023,
Accepted 18th February 2024

DOI: 10.1039/d3tb02748a

rsc.li/materials-b

Conductive hydrogel sensors have attracted attention for use in human motion monitoring detection, but integrating excellent biocompatibility, mechanical, self-adhesive, and self-healing properties, and high sensitivity into a hydrogel remains a challenge. In this work, a novel multifunctional conductive particle was designed and added to a polyacrylamide (PAM) matrix to prepare the hydrogel. It is worth noting that with the addition of polydopamine@poly(3,4-ethylenedioxythiophene) (PDA@PEDOT), the PAM/PDA@PEDOT hydrogel (PAPP hydrogel) showed excellent mechanical properties and high adhesion strength on different substrate surfaces. Meanwhile, the PAPP hydrogel shows outstanding self-healing properties, the mechanical properties of PAPP hydrogel broken from the middle recovered 92% tensile strength and 95% elongation at break after 12 h, respectively. Furthermore, assembled as strain wireless sensors, the PAPP sensor displays high sensitivity, where the gauge factor (GF) is 2.82, which can be used to accurately detect human facial micro-expressions and movements. Overall, the PAPP hydrogel with excellent mechanical, self-adhesive, and self-healing properties, and high sensitivity, demonstrated promise for use in wearable devices and bionic skins.

Introduction

Flexible sensors have garnered tremendous attention in the fields of human–machine interfaces, electronic skin, and wearable electronic devices, for their advantages of flexibility and biocompatibility.[1–5] Among them, conductive hydrogels have attracted extensive research interest because of their advantages of excellent toughness, high conductivity, high sensitivity, and fast response. Usually, most conductive hydrogels are prepared by combining hydrogel substrates with conductive nanomaterials (nanowires, carbon nanotubes) or intrinsically conductive polymers (polyaniline, sodium polystyrene sulfonate).[6–10] However, particle deposition and poor interfacial compatibility reduce the mechanical and electrical properties of conductive hydrogels.[11–13] Therefore, there is an urgent imperative to improve the dispersibility of the conductive nanofillers.

Moreover, self-adhesiveness is an attractive property of conductive hydrogels, which need to be worn or attached to the skin when used as flexible sensors.[14–17] The poor adhesion between the electronics and the soft body may reduce the sensitivity of the hydrogel. In addition to these properties, conductive hydrogels lack the desirable property of self-healing which limits its application in sensors.[18–22] Self-healing hydrogels are prepared by introducing dynamic and reversible bonds into hydrogel networks that can self-heal in response to damage and restore their original structure and properties, thereby improving the reliability and safety during use and extending its service life.[23–27] Sun *et al.* synthesized PEDOT:PSS-Poly(AAM-MAA) conductive hydrogel (PPAM) with good transparency and adhesion performance by using a semi-interpenetrating network (SIPN), but the breaking stress and elongation at break were only 68 kPa and 129%, respectively, which did not meet the requirements for the strain sensor for mechanical properties.[6] To sum up, the combination of high mechanical properties, self-adhesion, self-healing, and high sensitivity causes a problem for conductive hydrogels to meet the requirements of flexible wearable devices.

[a] Department of Critical Care Medicine, West China Hospital, Sichuan University, Chengdu, 610041, China. E-mail: huchenggong@scu.edu.cn
[b] College of Biomass Science and Engineering, Sichuan University, Chengdu, 610065, China
[c] Department of Cardiovascular Surgery, West China Hospital, Sichuan University, Chengdu, 610065, China
[d] West China School of Basic Medical Sciences and Forensic Medicine, Sichuan University, Chengdu 610041, P. R. China
[e] Qingdao Research Institute of Sichuan University, Qingdao 266200, P. R. China

† Electronic supplementary information (ESI) available. See DOI: https://doi.org/10.1039/d3tb02748a

‡ The authors contributed equally to this work.

Poly(3,4-ethylenedioxythiophene) (PEDOT) is widely used in bioelectronics due to its high electrical conductivity. However, the hydrophobicity of the inherent chemical structure hinders the dispersion of PEDOT in hydrogels, which is not conducive to the construction of a uniform conductive network in hydrogels and limits its application in the field of conductive hydrogels.[28–31] Recently, mussel-inspired polydopamine (PDA) has been widely studied for its extensive use in hydrophilic modification. In addition, the catechin groups in PDA serve as multifunctional sites that imbue biomaterials with various functions such as adhesion, self-healing, and antioxidant properties. Therefore, the mussel-inspired chemical mechanism may open up a new way to design multifunctional conductive hydrogels. Han *et al.* introduced graphene oxide (GO) into the PDA solution, and the entangled rGO of PDA was uniformly dispersed and interlaced to form electronic pathways, and the remaining unreduced GO and PDA chains interacted with the polyacrylamide (PAM) network by non-covalent interactions to prepare a conductive, stretchable, self-adhesive and self-healing hydrogel.[32] Jia *et al.* extracted silk microfibers (mSF) from raw silk with the help of polydopamine and then deposited poly(3,4-ethylenedioxythiophene) (PEDOT) on its surface to prepare ultra-long conductive filament microfibers, which were produced as conductive mSFs and used to fabricate conductive flexible sericin protein patches.[2] Inspired by the hydrophilic modification of PDA and its function as a molecular template, Yao *et al.* introduced PDA to guide the one-dimensional growth of pyrrole (Py) in the form of a molecular template, resulting in the formation of PDA-PPy nanofibers, which greatly improved the dispersion of polypyrrole (PPy) in the hydrogel matrix.[33] Jing *et al.* found that talcum powder could induce partial oxidation of dopamine, and the PDA-modified talcum powder particles were evenly dispersed in the PAM hydrogel, which led to a significant improvement in the mechanical properties and adhesion of the conductive hydrogel.[34] Thus, to take advantage of the mussel-inspired strategy, we designed a simple method to modify hydrophobic PEDOT with PDA to prepare multifunctional conductive nanoparticles (NPs) and to introduce them into hydrogels.

In this work, a PAM/PDA@PEDOT hydrogel (PAPP hydrogel) sensor with high mechanical, self-adhesive and self-healing properties, and high sensitivity was successfully designed and fabricated by introducing PDA@PEDOT into a polyacrylamide (PAM) hydrogel network (Scheme 1). In this study, the catechol group on the PDA layer acts as the active site to induce PEDOT deposition to form conductive particle PDA@PEDOT, which greatly improves the dispersion of PEDOT in the hydrogel matrix. In the next step, the PAPP hydrogel was successfully prepared by adding the multifunctional conductive particle PDA@PEDOT to the PAM matrix. The hydrogels have excellent mechanical, self-adhesive, and self-healing properties, and high sensitivity. The excellent versatility of the PAPP hydrogels is mainly attributed to the introduction of nanoparticles. These conductive NPs are uniformly distributed in the hydrogel and

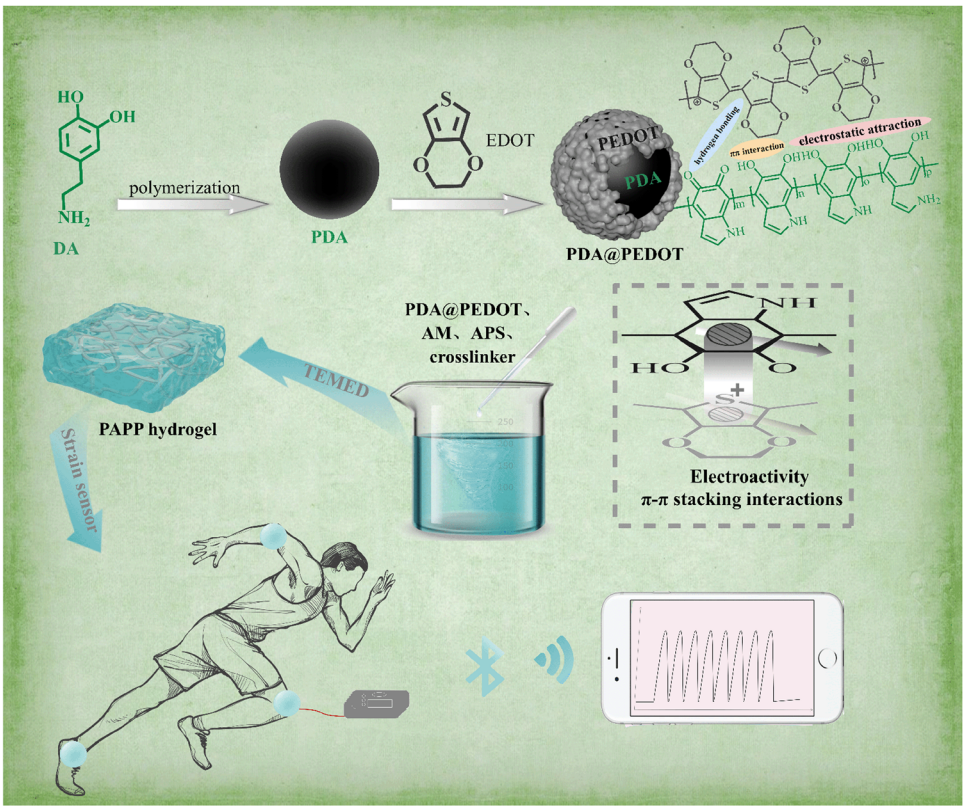

Scheme 1 Scheme illustrating the preparation process of the PAPP hydrogels.

introduce non-covalent interactions in the chemically crosslinked PAM hydrogel. Finally, the conductive hydrogel PAPP was assembled into sensors to monitor human movement and facial micro-expressions. This work provides a general strategy to construct hydrogel-based multifunctional sensors as next-generation wearable devices for real-time monitoring.

Experiments

Materials

Acrylamide (AM), dopamine (DA) and trihydroxymethyl aminomethane (Tris) were purchased from Sigma-Aldrich. Ammonium persulfate (APS, initiator), *N,N,N′,N′*-tetramethylethylenediamine (TEMED, catalyst), and 3,4-ethylenedioxythiophene (EDOT) were obtained from Aladdin Reagent Inc. (Shanghai, China).

Preparation of PDA@PEDOT

In the first step, dopamine suspension (0.1 M) was put into a round-bottomed beaker, and adjusted to a pH of 8.5 by dropwise addition of Tris buffer, which was stirred at room temperature for 4 h. EDOT (0.1 M) was dispersed in a mixture of ethanol and deionized water (ethanol:deionized water = 3 : 1), which was then added to the PDA reaction mixture and stirred vigorously for 30 min until the EDOT was evenly dispersed. Subsequently, $FeCl_3$ solution was dropped into the mixture and stirred at room temperature for 24 h.[5,35] Finally, the obtained mixture was centrifuged and washed several times with deionized water and ethanol to obtain PDA-modified PEDOT particles (PDA@PEDOT).

Preparation of PAM/PDA@PEDOT (PAPP) hydrogels

The PDA@PEDOT (0.2 wt%, 0.4 wt%, 0.6 wt%, 0.8 wt%, and 1 wt%) was mixed with the appropriate amount of water. Then, AM (4.0 g), the prepared macromolecular crosslinker polyurethanes (MPU)[3] referred to in our previous work (1.0 g), APS (40 mg), and TEMED (10 μL) were dissolved into the above solution followed by 20 min of stirring to obtain a uniform solution. Finally, the solution was ultrasonically treated to remove the bubbles and transferred to a PTFE mold and placed at ambient temperature for 24 h to obtain the PAPP hydrogels (labeled as PAPP-*x*, where *x* is the mass fraction of PDA@PEDOT.

Characterization

The microstructures were observed using a Fourier transform infrared spectroscope (FT-IR, Nicolet, USA). The X-ray photoelectron spectroscopy (XPS) spectra were recorded on an XSAM 800 instrument (Kratos) to determine the chemical composition. Scanning electron microscopy using a JSM-7500F instrument (Jeol, Japan), and energy dispersive X-ray spectroscopy (EDX) were used to determine the morphology of the PDA@PEDOT particles and the internal morphology and element distribution of the hydrogels. A CEL-S500 xenon lamp with a power density of 250 mW cm^{-2} (Beijing Zhongjiao Jinyuan Technology Co., Ltd) was used to test the photothermal effect.

The mechanical properties and peeling performance were tested using a universal tensile testing machine (Instron Electron Instrument Co., Ltd, USA) at room temperature. The hydrogels were shaped into a dumbbell shape (width of 4 mm, thickness measured before the tensile testing) to carry out the single tensile test and cyclic test at 100 mm min^{-1}. For the compressive test, cylindrical compression samples were shaped with a diameter of 20 mm and a height of 30 mm with a compression speed of 10 mm min^{-1}. In the same Instron 5967 tensile testing machine, the hydrogel samples were placed between PDMS, wood and pig skin substrate, and the adhesion properties of the hydrogel samples (40.0mm × 40.0mm × 2.0mm) were tested.

The PAPP hydrogels with different PDA@PEDOT contents were tested using a MCR 302 rheometer (Anton Parr, Germany), with a gap height of 1 mm at 25 °C. The fixed frequency of the dynamic strain sweep experiment is 10 Hz, and the fixed strain of the frequency scanning test is 0.1%. Cyclic strain time scanning measurements were performed with strain steps shifting between 1% and 100% at a constant frequency of 10 Hz. The electronic chemical properties were investigated using a multifunctional wireless system (Hangzhou LinkZill Technology Co., Ltd).

In order to investigate the *in vitro* cytotoxicity of the hydrogels, 100 μL of L929 cell suspension (KG087, KeyGEN BioTECH, Nanjing, China) were inoculated into 96-well plates at a density of 5000 cells per well at 37 °C and then left under 5% CO_2 for 24 h. Subsequently, fresh Dulbecco's modified Eagle's medium (DMEM) cell cultures containing PAM and PAPP hydrogels were transferred to each well and after growing for 1, 3, 5 and 7 days, the cells were counted using Cell Counting Kit-8 (CCK-8, Dojindo, Shanghai, China) assays. At the same time, live and dead cell assays were used to assess cell viability. The L929 cells were then cultured with a mixture of hydrogel and DMEM. A mixed buffer containing 2 μM of calcein AM and 4.5 μM of propidium iodide (200 μL) was added and removed after 30 min. Finally, fluorescence images of the cells were captured using confocal laser scanning microscopy.

Results and discussion

Synthesis and characterization

In this study, the hydrophobic PEDOT was first modified by PDA using electrostatic attraction and π–π interaction, and then added to the PAM matrix to prepare hydrogel. Fig. 1, shows the morphology of PEDOT, PDA, and PDA@PEDOT observed by scanning electron microscopy. The SEM images show that the PEDOT and PDA were strip shaped and spherical shaped, respectively. Fig. 1c shows PDA@PEDOT with a core–shell structure, demonstrating the successful introduction of PEDOT onto the PDA NPs surface. The Tyndall effect occurred when infrared rays passed through the PDA@PEDOT colloidal solution, which indicated that PDA@PEDOT particles are uniformly dispersed. In addition, as shown in Fig. 1d and e, the S element (red) was uniformly distributed on the spherical surface and had a mass fraction of 8.35%, which also proves the successful introduction of PEDOT.

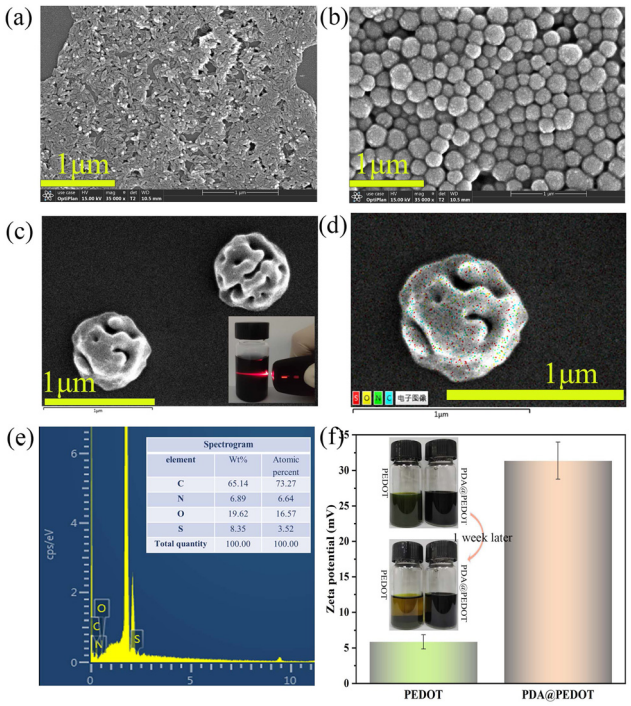

Fig. 1 SEM images of (a) PEDOT, (b) PDA, and (c) PDA@PEDOT; (d) mapping and (e) EDX images of PDA@PEDOT particles; (f) The zeta potentials and images of the PEDOT and PDA@PEDOT dispersions.

The zeta potential is associated with the surface charge of nanoparticles and can be used to determine the stability of colloidal dispersion systems.[36,37] The absolute value of the zeta potential is positively correlated with the mutual repulsion between nanoparticles. As shown in Fig. 1f, the zeta potential of the PDA@PEDOT dispersion increased from 5.87 mV to 31.37 mV after the modification of the PDA. The stability of the PDA@PEDOT dispersion is obviously better than that of pure PEDOT.

In this work, we successfully prepared a novel PAPP conductive hydrogel by introducing PDA@PEDOT into the polyacrylamide (PAM) hydrogel network. As shown in Fig. 2a, FT-IR was employed to determine the chemical structures of PAM, PDA@PEDOT, and the PAPP hydrogels For PDA@PEDOT, quinoid type C–C vibrations were found at 1460 cm^{-1} and are attributed to the thiophene ring. The characteristic peaks of C–O–C stretching vibrations were found at 1173 cm^{-1} and 1001 cm^{-1}, and the characteristic peaks associated with the C–S vibrations of the thiophene ring were found at 973 cm^{-1} and 850 cm^{-1}.[5,38,39] Furthermore, it exhibited a wide and strong band between 3400 cm^{-1} and 3000 cm^{-1} due to the O–H bond of the DA molecule. The characteristic peaks of the C–O–H bond asymmetric bending vibration were seen at 1320 cm^{-1}.[40,41] According to these results, it was proved that the PDA@PEDOT particles had been successfully synthesized. For PAM and PAPP, the characteristic peak of the $-CONH_2$ group was observed at 1661 cm^{-1} (C=O bending vibration) and 2920 cm^{-1} ($-CH_2$ stretching vibration), and the characteristic peak at 3421 cm^{-1} was attributed to the N–H stretching vibration.[42–44] In addition, the characteristic peaks of PDA@PEDOT were also found in PAPP, which indicated that the PAPP hydrogel had been prepared successfully. Further, the XPS surveys were applied to validate the surface elements and the valence states of PDA@PEDOT, the PAM hydrogels, and the PAPP hydrogels. As shown in Fig. 2b, the peak at about 163 eV in the spectrum of PAPP was assigned to S. This indicated that PEDOT had been introduced into the PAPP hydrogel. In Fig. 2c, the XPS image of S2p showed two separate peaks in the range of 163 eV and 164 eV, which were assigned to $S2p_{1/2}$ and $S2p_{3/2}$, respectively.[45–47]

The morphological characteristics of the PAM and PAPP hydrogels after freeze-drying were observed using SEM-EDX. As shown in Fig. 3, the PAPP hydrogel surface showed a more uniform pore size, and a thicker and smoother pore wall compared with the pure PAM hydrogel, indicating that the PAPP hydrogel structure was more stable under the action of an external force. As a result, the PAPP hydrogels show a uniform honeycomb porous structure, which is suitable for use as wearable sensors with large deformation over long periods of time. Furthermore, the element distribution of the PAPP hydrogel was analyzed by EDX element mapping. In Fig. 3c–g, the EDX element mapping showed that sulfur (yellow), nitrogen (indigo), oxygen (green), and carbon (red) elements were evenly distributed on the surface of the PAPP hydrogel.

Mechanical performances

Generally, it is difficult for the mechanical properties of conventional gel structures to meet the requirements of long-term applications. Therefore, the PDA@PEDOT particles were introduced into the hydrogel to improve the mechanical properties. As shown in Fig. 4, the PAPP hydrogels went through several external stimuli, including stretching (stretching rate >3000%), twisting, tying, and compression. It is worth noting that the PAPP hydrogel could be rapidly restored to its original state after undergoing huge deformation, implying that the introduction of PDA@PEDOT which causes the fragile hydrogels to have a high mechanical strength and elasticity.

The effect of PDA@PEDOT content on the mechanical properties of hydrogels was also investigated. As shown in Fig. 5a and b, the PAM hydrogels showed poor elongation at break (850%) and tensile strength (317 kPa) before the addition of PDA@PEDOT. As the PDA@PEDOT content increased from 0 to 0.8%, the elongation at break of the PAPP hydrogels increased from 850% to 3383.5%, and the tensile strength decreased from 317 kPa to 187 kPa, which was attributed to the homogeneous dispersion of hydrophilic PDA@PEDOT, and the interfacial interaction between PAM and PEDOT, and the incorporation of PDA@PEDOT further increased the elongation at break. When the PDA@PEDOT content exceeds 0.8%, the mechanical strength and elongation at break of the hydrogel decreased simultaneously. As the content of PDA@PEDOT increased, the catechol groups on the polydopamine chain delayed the polymerization of PAM in the presence of the APS initiator, and the degree of crosslinking of the hydrogel network decreased. Therefore, the PAPP-0.8% hydrogel displayed the highest elongation at break (3383.5%) when compared with

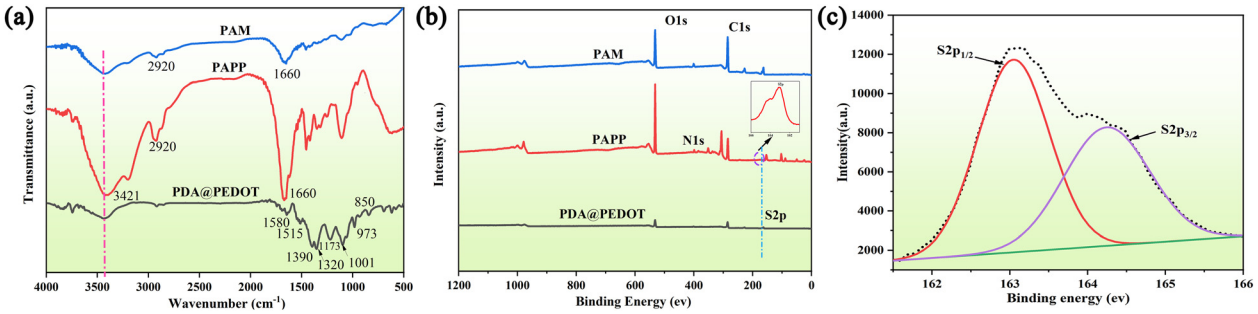

Fig. 2 (a) The FT-IR spectra of PAM, PDA@PEDOT, and PAPP hydrogels; (b) the XPS spectra of PAM, PDA@PEDOT, and PAPP hydrogels; (c) the S2p images of PAPP.

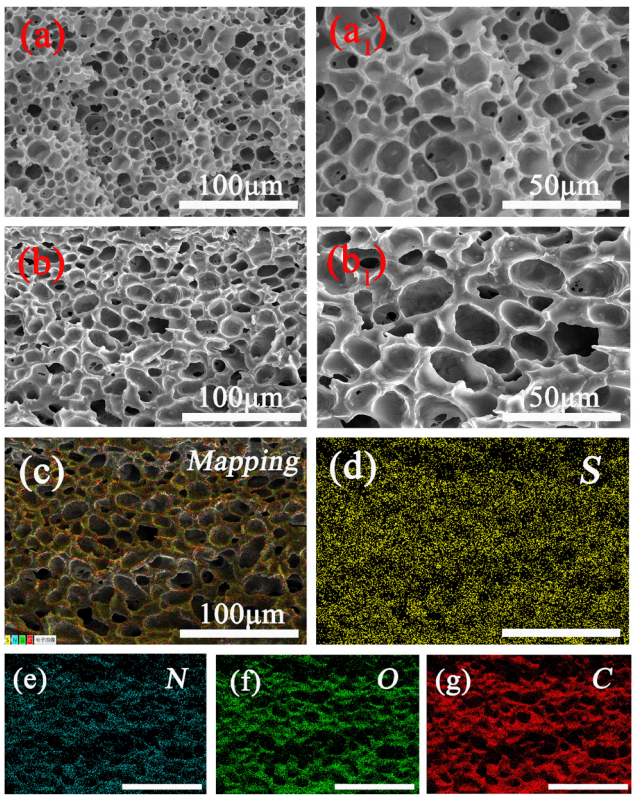

Fig. 3 The SEM images of the PAM hydrogel (a) and (a_1), the PAPP hydrogel (b) and (b_1), and the corresponding EDX element mapping of the PAPP hydrogel (c), including sulfur (d), nitrogen (e), oxygen (f), and carbon (g).

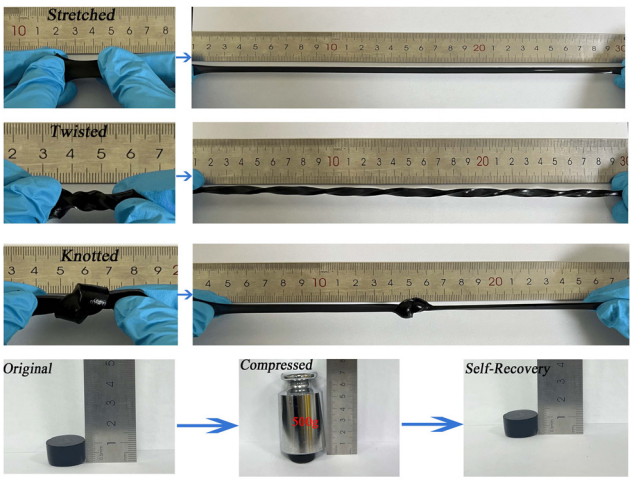

Fig. 4 Photograph of PAPP hydrogels being tested against external stimuli processes (stretched, twisted, knotted, and compressed).

the other PAPP hydrogels, and this was used for the tensile cycling tests. As shown in Fig. 5c and d, the loading–unloading tensile curves showed no remarkable strain residue. After five cycles of tensile testing at a 200% strain ratio, the self-recovery rate was up to 95.8%. Therefore, the tensile properties of the PAPP hydrogel can fully meet the needs of wearable devices.

As shown in Fig. 5e and f, the influence of the PDA@PEDOT content on the compressive strength of PAPP hydrogel was further explored. Under 60% compression, as the PDA@PEDOT content increased from 0 to 1%, the compressive strength of the hydrogel decreased from 103.1 kPa to 26.8 kPa. Due to the introduction of PDA@PEDOT, the crosslinking density of PAM and crosslinking agent MPU decreased, thus reducing the compression strength of the hydrogel. As shown in Fig. 5g and h, it is worth noting that the compressive strength of the hydrogel is only 30.8 kPa, but the self-recovery rate is as high as 95.7% after 50 compression cycles with a strain of 60%, indicating that the PAPP hydrogel exhibits excellent structural self-recovery properties.

Rheological properties and self-healing behaviors

The viscoelastic properties of the prepared PAPP hydrogels with different PDA@PEDOT concentrations were determined by amplitude scanning and frequency scanning. As seen in Fig. 6a, the storage modulus (G') and loss modulus (G'') remained unchanged within the range of 0.1–20% strain, which is the linear viscoelastic region of the hydrogel. It was observed that the G' of each hydrogel decreased after exceeding the linear viscoelastic region, and indicated the destruction of the internal structure had occurred.[48,49] In addition, with the increase of the PDA@PEDOT concentration, G' gradually decreased, which was due to the introduction of the PDA@PEDOT, and the crosslinking density of the PAM and MPU also

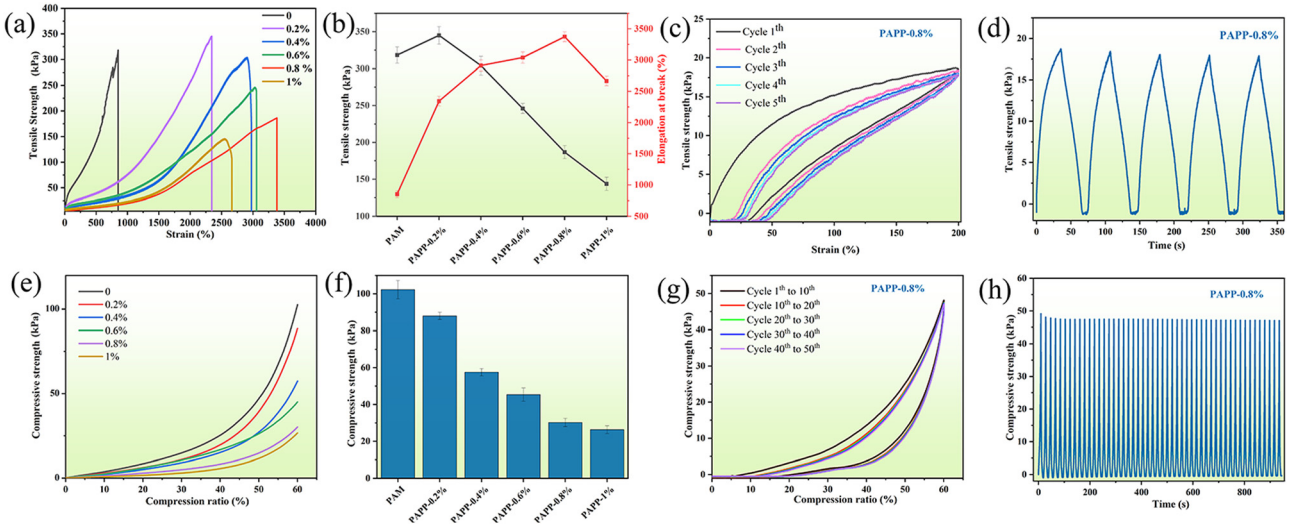

Fig. 5 Mechanical properties of hydrogels. (a) Stress–strain curves and (b) the maximum tensile strength and elongation at break of hydrogels; stress data of five cycles of the PAPP-0.8% hydrogel at 200% (c) stress–strain curves and (d) the maximum tensile strength; (e) compression stress–strain curves and (f) the maximum compressive strength of the PAPP hydrogels at 60%; compressive data of 50 cycles of the PAPP-0.8% hydrogel at 60% (g) compressive–strain curves and (h) the maximum compressive strength.

decreases, thus reducing the stiffness of the hydrogel. As shown in Fig. 6b, the frequency scanning test was used to investigate the effect of PDA@PEDOT concentration on the viscoelasticity of the hydrogel. It was observed that the G' of all the hydrogels exceeds G'', demonstrating that the PAPP hydrogel maintains an ideal elasticity over the test frequency range. In this frequency range, G' decreases with the increasing PDA@PEDOT concentration, which was due to the decrease of the degree of crosslinking of the other crosslinking network caused by the introduction of PDA@PEDOT. The degree of crosslinking of the PAM network is the main factor for the stiffness of the hydrogel system.

In addition, the self-recovery performance is crucial for strain sensors. In Fig. 6c, cyclic strain-time scanning was used to test the cyclic recovery performance of the hydrogels, step-strain measurements were performed between 0.1% and 100% strain to explore the rupture and recovery of the shear moduli of the hydrogels. After five cycles, the PAPP hydrogel has a very high modulus recovery (98.94%), indicating that the PAPP hydrogel has excellent structural stability. In addition, when the strain of the hydrogel is 0.1%, G' is higher than G'', indicating that hydrogel is a crosslinked hydrogel network. When the strain is 100%, G' drops sharply from 6650 Pa to 2890 Pa, which was lower than G'', showing viscosity, and indicating an instantaneous transition from quasi-solid to quasi-liquid. This is attributed to the collapse of the hydrogel network under large strains and the transformation into a solution state. When the strain was restored to 0.1%, G' and G'' immediately returned to almost the same initial value within a few seconds, indicating that the internal structure of the hydrogel had been reconstructed. The self-healing behavior was completely reversible and was repeated in the cycle test, which further confirmed that the PAPP hydrogel had excellent rapid self-healing performance. As shown in Fig. 6d, compared with the original hydrogel, the mechanical properties of PAPP hydrogel after 12 h recovered 92% of their tensile strength and 95% of their elongation at break. These results indicate that the PAPP hydrogel has an excellent healing ability, which can greatly prolong its service life and ensure its reliability as a strain sensor. The PAPP hydrogels show excellent self-healing properties, which are attributed to reversible interactions between the phenolic hydroxyl groups on PDA and the amino groups on PAM, the hydrogen bonding between PDA, and the π–π stacking that reconfigure the hydrogel network.[50–52] Therefore, the PAPP self-healing hydrogels show great potential for applications in smart sensors and wearable electronic devices.

Photothermal effect of PAPP hydrogels

The hydrogel-based electronic skin can be used as a personal heat management system due to its excellent photothermal effect. Therefore, the photothermal conversion performance of the PAPP hydrogel was studied by irradiating it with a xenon lamp and recording the temperature change of the sample with a thermal imager. As shown in Fig. 7b, the temperature–time curve shows that the temperature of the sample continued to rise and finally stabilized at about 107 °C under xenon lamp irradiation, and then gradually dropped to an ambient temperature after the xenon lamp was turned off. In addition, Fig. 7c shows that when the PAPP hydrogels were heated photothermally from ambient temperature to 60 °C and then cooled to room temperature, the five-cycle curve demonstrated the repeatability and long-term durability of the PAPP hydrogels for photothermal applications.

Adhesiveness of the PAPP hydrogels

In general, the hydrogel strain sensor described in the literature had no adhesive property and needs to be fixed with tape, which imposes additional stress on the sensor and creates

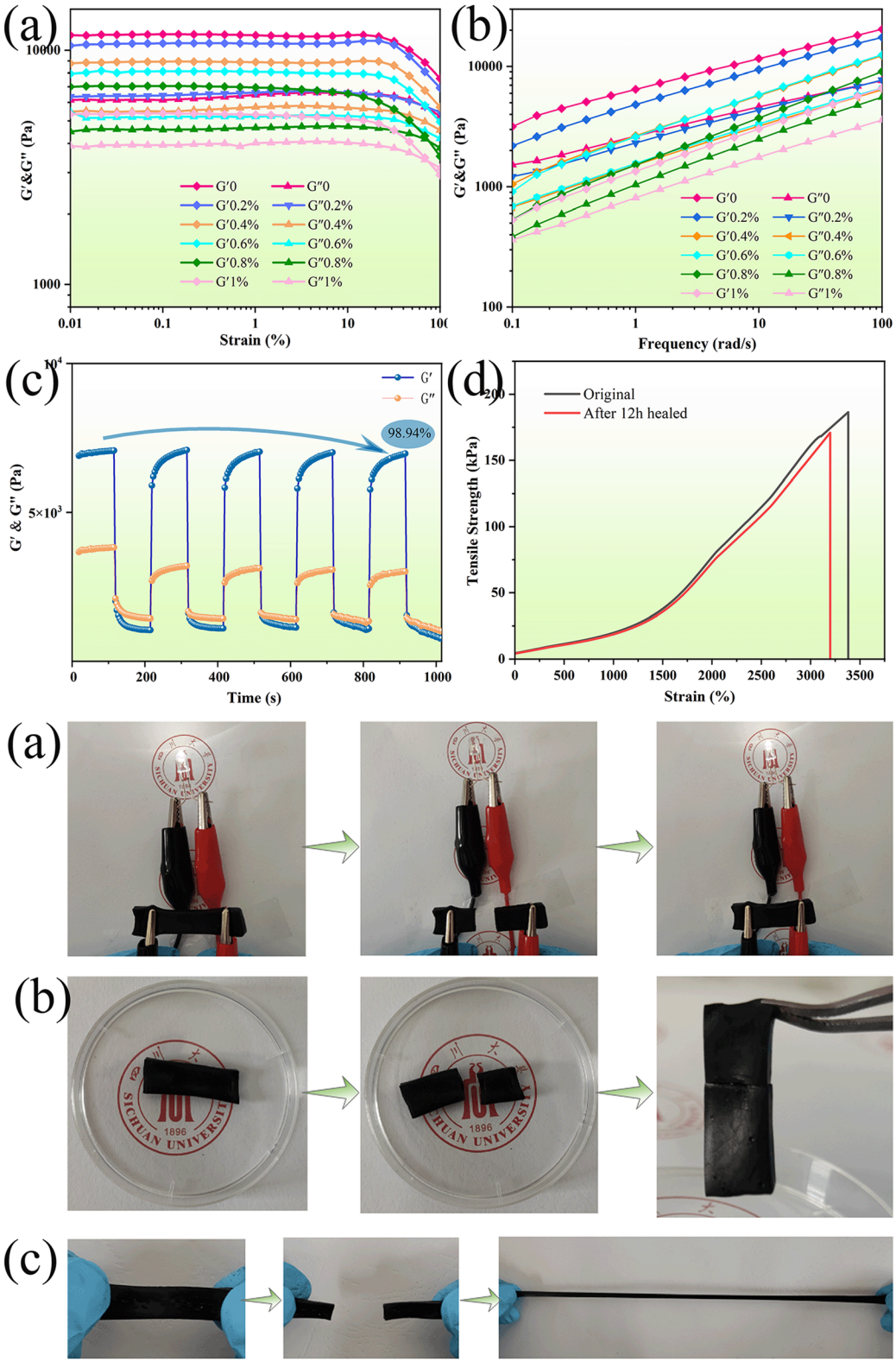

Fig. 6 Rheological properties of hydrogels with different contents of PDA@PEDOT. (a) Strain as the independent variable; (b) frequency as the independent variable; (c) The cyclic strain time sweep for the PAPP-0.8% hydrogel. (d) the stress–strain curves of PAPP-0.8% hydrogel before cutting and healing after 12 h.

unnecessary motion artifacts. As shown in Fig. 8a, the PAPP hydrogel has excellent adhesion properties and can firmly adhere to the surface of glass, rubber, plastic, wood, aluminum sheet, and pigskin. In addition, the PAPP hydrogel can also

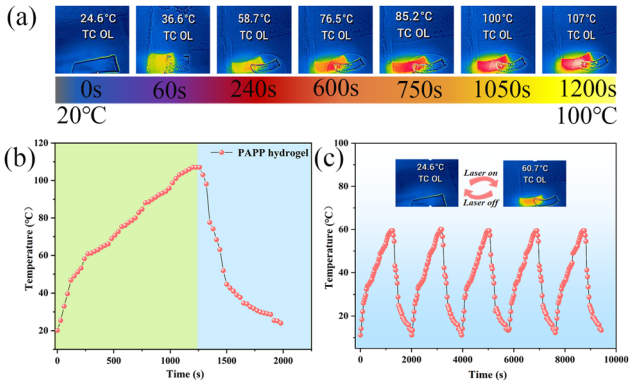

Fig. 7 (a) Infrared thermometer images of the PAPP hydrogel under xenon light irradiation; (b) heating and cooling curves of PAPP hydrogel under xenon light irradiation; (c) The photothermal conversion of PAPP hydrogel.

adhere firmly to two fingers under stretching, indicating that the hydrogel has excellent adhesion performance on the skin surface, which is a significant performance for a strain sensor.

Furthermore, the effect of the PDA@PEDOT concentration on the PAPP hydrogel adhesion was investigated using a lap shear test. As shown in Fig. 8b, the maximum adhesion strength of the pure PAM hydrogel is only 34.2 kPa. With the increase of PDA@PEDOT content from 2% to 6%, the adhesive strength of the PAPP hydrogel increased from 65.1 kPa to 96.1 kPa. When PDA@PEDOT content was 8%, the adhesive strength of the PAPP hydrogel decreased to 54.8 kPa. When the PDA@PEDOT content was 0.6%, the PAPP hydrogel showed the best adhesion performance. As shown in Fig. 8c, on the substrate surface of PDMS, pigskin, and wood, the adhesion strength values of the PAPP-0.6% hydrogels were 96.1 kPa, 120.3 kPa, and 172.5 kPa, respectively. Hydrogels can adhere for a long time due to the REDOX properties of the charge transfer from PEDOT to PDA between the catechol and quinone groups of PDA. As shown in Fig. 8e, the adhesion properties of the PAPP hydrogel on three substrates were measured over five cycles. It is worth noting that the PAPP hydrogels still showed an excellent adhesion performance when they were adhered for the fifth time. The PDA@PEDOT in the hydrogel network could realize the dynamic reaction between catechol groups and quinone groups, endowing the hydrogel with repeatable adhesiveness.[2,5]

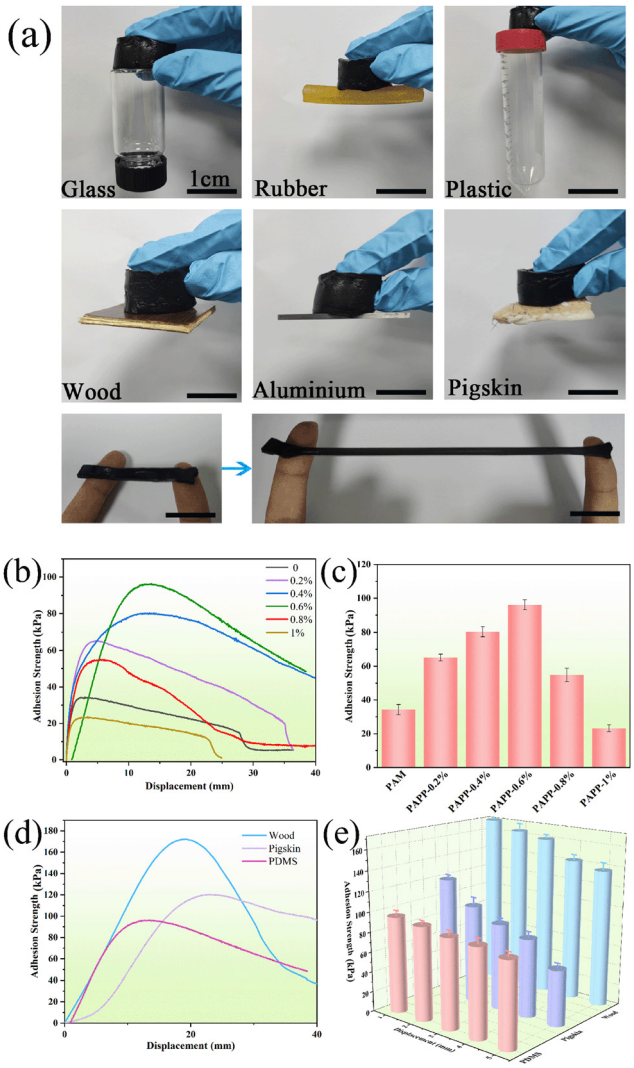

Fig. 8 Adhesive behaviors of the PAPP hydrogels. (a) Photographs of the PAPP hydrogels adhered on various polar substrates; (b) peel off curves of PAPP hydrogels with different PDA@PEDOT contents on the surface of PDMS; (c) the maximum adhesive strength of the PAPP hydrogels on the surface of PDMS; (d) peel off curves of the PAPP hydrogels on the surface of different materials (PDMS, pigskin, and wood); (e) cyclic adhesion properties of PAPP hydrogels on different substrates.

Sensing performance of the PAPP hydrogels

Generally, PDA can enhance the conductivity of conductive materials such as GO, PPy, and PEDOT due to the hybridization of PDA. Therefore, the PAPP hydrogel was assembled into a strain sensor (labeled as PAPP sensor). As shown in Fig. 9a, with the increase of strain, the change of relative resistance of the tension-relaxation cycle increases, and the signal is stable and repeatable. Interestingly, the hydrogel sensor is frequency-dependent, with the rate of change of resistance remaining consistent at different frequencies (Fig. 9a). Sensitivity is a vital parameter for evaluating strain sensors. As shown in Fig. 9c, in the strain range of 0–600% and 600–1000%, the gauge factors (GF) of the PAPP sensor were 1.71 and 2.82, respectively, indicating that the PAPP sensor showed outstanding strain sensitivity compared with most of the other hydrogel sensors reported. Furthermore, as shown in Fig. 9g, the brightness of the LED bulbs decreases when stretched and recovers rapidly when the stress is released, which also confirms the strain-sensitive behavior. As shown in Fig. 9d, the response time of the PAPP hydrogel was only 196 ms, which proved its excellent response speed. In Fig. 9f, the PAPP sensor was stretched and relaxed 200 times (fixed strain of 200%), and the signal was still stable and reliable. The schematic mechanism of the charge transfer process between PEDOT and PDA is shown in Fig. 9e, where the low ionization energy of PEDOT causes the oxidation of PEDOT by interaction with the catechol or quinone groups of

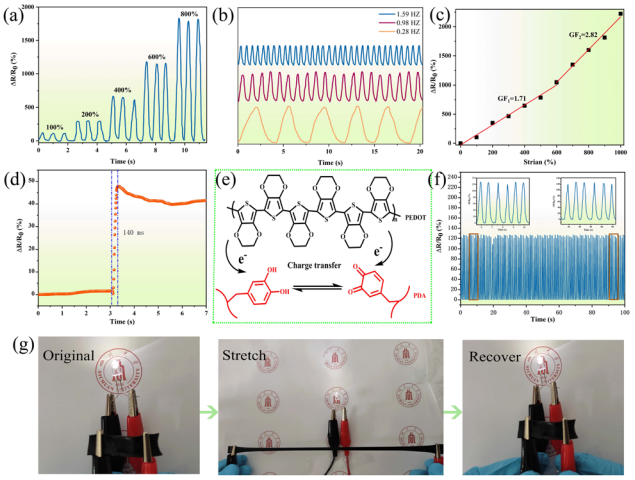

Fig. 9 (a) The evolution of the $\Delta R/R_0$ signals under 100%, 200%, 400%, 600%, and 800% strains; (b) cyclic stretching–relaxing under different frequencies; (c) sensitivity of strain sensors ranging from 0 to 1000%; (d) response speed of the PAPP strain sensor; (e) a schematic representation of charge transfer between PEDOT and the catechol and quinone groups of PDA; (f) cycling stability of the strain sensor; (g) the brightness of the LED light responding to the stretching of the PAPP hydrogel sensor.

PDA. The resulting catechol-to-quinone conversion becomes an electron acceptor due to the charge transfer between the catechol/quinone groups of PEDOT and PDA, and quinone structures are formed to enhance the electrical conductivity.

Human body movement monitoring

Due to the excellent sensing ability of the PAPP hydrogel within a wide range of strains and pressures, a skin-like sensor was designed as a wearable sensor to monitor human motion (labeled as PAPP sensors). The PAPP hydrogel was connected to a wireless system, which includes a microcontroller (MCU)

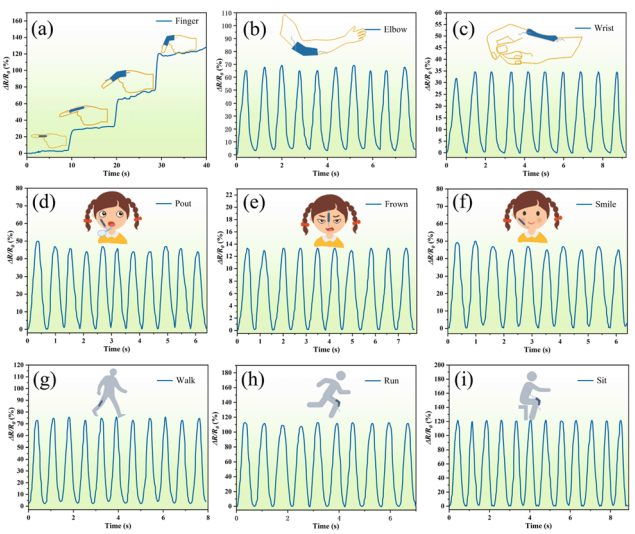

Fig. 10 The PAPP sensors for mechanotransduction signal applications: (a) finger bending; (b) elbow bending; (c) wrist bending; (d) pouting; (e) frowning; (f) smiling; (g) walking; (h) running, and (i) sitting.

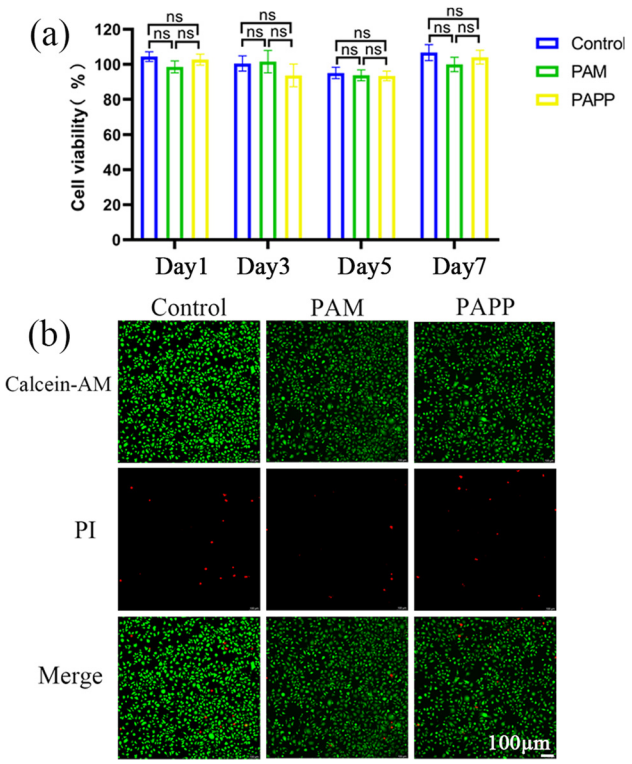

Fig. 11 (a) Effects of PAS and PAPP hydrogels on cell proliferation, n = 6, error bars indicate standard deviation, ns: not significant; (b) live/dead staining of cells treated with PAS and PAPP hydrogels (green for live cells, red for dead cells).

and an analog-to-digital converter (ADC). In Bluetooth wireless mode, the regular and stable detection data is presented in real-time on a smartphone. As displayed in Fig. 10, the PAPP sensor could be directly installed onto the human skin, and the wireless sensor could detect various human motions. As shown in Fig. 10a, the PAPP hydrogel sensor is used to detect the finger bending angle, and the relative resistance varies with the degree of finger bending. Furthermore, the relative resistance of the PAPP sensor can be monitored as it is attached to the elbow, wrist, face, or legs as shown in Fig. 10b–d). The results show that the hydrogel sensor can be used to detect both micro-expressions (pouting, frowning, and smiling) and large body movements (walking, running, and sitting) due to its high sensitivity. The above results revealed that the PAPP sensors have great potential in wireless sensors and remote sensing. A detailed comparison of PASU-Zn with the reported hydrogels is shown in Table S1 (ESI†).

Biocompatibility

The wearable sensors need to be in direct contact with the skin tissue, so biocompatibility is a guarantee of its safe usage. Therefore, the biocompatibility of the PAPP hydrogel was assessed using CCK-8 and live-death staining tests. As shown in Fig. 11a, the effect of the PAPP hydrogel on the viability of fibroblasts (L929) was evaluated by CCK-8 testing. After the extracts of PAM and PAPP hydrogels were incubated with cells,

the cell viability remained above 90% after 1, 3, 5, and 7 days, indicating that the two hydrogels had excellent cytocompatibility. As shown in Fig. 11b, the live/dead staining results on day 3 showed that a small number of cells in each group were red, but the vast majority of cells were green, further indicating that these hydrogels had excellent cytocompatibility. Therefore, the excellent biocompatibility of PAPP hydrogels broadens their practical applications as wearable strain sensors.

Conclusion

In summary, we successfully prepared a novel hydrogel sensor by introducing multifunctional conductive particles, PDA@PEDOT, into the PAM matrix, the hydrogel sensors simultaneously exhibited excellent biocompatibility, mechanical properties, self-adhesion, self-healing, and high sensitivity for human facial micro-expressions and motion detection. In conclusion, it provides a rational strategy for developing hydrogel sensors with outstanding tensile properties, high sensitivity, remarkable self-adhesive properties, and excellent self-healing properties.

Data availability

Data will be made available on request.

Conflicts of interest

The authors declare that they have no known competing financial interests or personal relationships that could have appeared to influence the work reported in this paper.

Acknowledgements

This project was supported by the Sichuan Science and Technology Program (2022YFG0273, 2023YFS0168, 2023NSFSC0308, 24QYCX0367), 1.3.5 project for disciplines of excellence, West China Hospital, Sichuan University(ZYGD23012). The authors also thank Zeliang Wei and Erhui Ren for their assistance with the experimental testing.

Notes and references

1 R. Kim and Y. Nam, *J. Neurosci. Methods*, 2019, **326** 108369.
2 Z. Jia, J. Gong, Y. Zeng, J. Ran, J. Liu, K. Wang, C. Xie, X. Lu and J. Wang, *Adv. Funct. Mater.*, 2021, **31**, 2010461.
3 H. Wang, X. Li, Y. Ji, J. Xu, Z. Ye, S. Wang and X. Du, *J. Mater. Chem. B*, 2022, **10**, 2933–2943.
4 J. Zou, X. Jing, Z. Chen, S. J. Wang, X. S. Hu, P. Y. Feng and Y. J. Liu, *Adv. Funct. Mater.*, 2023, 33.
5 D. Gan, Z. Huang, X. Wang, L. Jiang, C. Wang, M. Zhu, F. Ren, L. Fang, K. Wang, C. Xie and X. Lu, *Adv. Funct. Mater.*, 2019, **30**, 1907678.
6 X. Sun, Z. Qin, L. Ye, H. Zhang, Q. Yu, X. Wu, J. Li and F. Yao, *Chem. Eng. J.*, 2020, **382**, 122832.
7 S. He, X. Sun, Z. Qin, X. Dong, H. Zhang, M. Shi, F. Yao, H. Zhang and J. Li, *Adv. Mater. Technol.*, 2021, **7**, 2101343.
8 S. Wang, Y. Fang, H. He, L. Zhang, C. A. Li and J. Ouyang, *Adv. Funct. Mater.*, 2020, **31**, 2007495.
9 Z. Ma, Z. Liu, J. Zou, H.-Y. Mi, Y. Liu and X. Jing, *ACS Sustainable Chem. Eng.*, 2023, **11**, 10496–10508.
10 L. Jiang and X. Lu, *Mater. Chem. Front.*, 2021, **5**, 7479–7498.
11 Z. Zhang, Z. Zheng, Y. Zhao, J. Hu and H. Wang, *Compos. Sci. Technol.*, 2021, **213**, 108968.
12 L. Wang, T. Xu and X. Zhang, *TrAC, Trends Anal. Chem.*, 2021, **134**, 116130.
13 Z. Deng, R. Yu and B. Guo, *Mater. Chem. Front.*, 2021, **5**, 2092–2123.
14 J. Xiang, R. Zhu, S. Lang, H. Yan, G. Liu and B. Peng, *Chem. Eng. J.*, 2021, **409**, 128291.
15 C. Hu, L. Long, J. Cao, S. Zhang and Y. Wang, *Chem. Eng. J.*, 2021, **411**, 129329.
16 S. Lu, X. Zhang, Z. Tang, H. Xiao, M. Zhang, K. Liu, L. Chen, L. Huang, Y. Ni and H. Wu, *Chem. Eng. J.*, 2021, **417**, 129329.
17 S.-J. Wang, Z. Chen, X. Hu, J. Zou, Z. Xie, H.-Y. Mi, Z.-H. Liu, Z. Zhang, Y. Shang and X. Jing, *J. Mater. Chem. C*, 2022, **10**, 11914–11923.
18 W. Zheng, C. Chen, X. Zhang, X. Wen, Y. Xiao, L. Li, Q. Xu, F. Fu, H. Diao and X. Liu, *Surf. Coat. Technol.*, 2021, **406**, 126644.
19 L. Jiang, Z. Liu, J. Liu, S. He, X. Wu and W. Shao, *Ind. Crops Prod.*, 2023, **192**, 116083.
20 Y. Wang, L. Sun, G. Chen, H. Chen and Y. Zhao, *ACS Nano*, 2022, **17**, 1437–1447.
21 H. Bai, D. Chen, H. Zhu, S. Zhang, W. Wang, P. Ma and W. Dong, *Colloids Surf., A*, 2022, **648**, 129205.
22 Z. Deng, Y. Guo, X. Zhao, P. X. Ma and B. Guo, *Chem. Mater.*, 2018, **30**, 1729–1742.
23 F.-L. Yi, F.-C. Meng, Y.-Q. Li, P. Huang, N. Hu, K. Liao and S.-Y. Fu, *Composites, Part B*, 2020, **198**, 108246.
24 Z. Wang, M. Bu, K. Xiu, J. Sun, N. Hu, L. Zhao, L. Gao, F. Kong, H. Zhu, J. Song and D. Lau, *Nano Energy*, 2022, **104**, 107978.
25 M. Yang, X. Ren, T. Yang, C. Xu, Y. Ye, Z. Sun, L. Kong, B. Wang and Z. Luo, *Chem. Eng. J.*, 2021, **418**, 129483.
26 Z. Xie, Z. Chen, X. Hu, H.-Y. Mi, J. Zou, H. Li, Y. Liu, Z. Zhang, Y. Shang and X. Jing, *J. Mater. Chem. C*, 2022, **10**, 8266–8277.
27 X. Jing, P. Feng, Z. Chen, Z. Xie, H. Li, X.-F. Peng, H.-Y. Mi and Y. Liu, *ACS Sustainable Chem. Eng.*, 2021, **9**, 9209–9220.
28 C. Zhou, T. Wu, X. Xie, G. Song, X. Ma, Q. Mu, Z. Huang, X. Liu, C. Sun and W. Xu, *Eur. Polym. J.*, 2022, **177**, 111454.
29 R. Yan, Y. Yan, J. Gong and J. Ma, *Mater. Res. Express*, 2019, **6**, 055322.
30 J. Zhao, J. Xiong, Y. Ning, J. Zhao, Z. Wang, L. Long, H. He, J. Gou, T. Yin, X. Tang and Y. Zhang, *Eur. J. Pharm. Biopharm.*, 2023, **185**, 44–54.
31 Z. Zhao, R. Fang, Q. Rong and M. Liu, *Adv. Mater.*, 2017, **29**, 1703045.
32 L. Han, X. Lu, M. Wang, D. Gan, W. Deng, K. Wang, L. Fang, K. Liu, C. W. Chan, Y. Tang, L. T. Weng and H. Yuan, *Small*, 2017, 13.

33 B. Yao, Z. Ye, X. Lou, Q. Yan, Z. Han, Y. Dong, S. Qu and Z. Wang, *ACS Appl. Mater. Interfaces*, 2022, **14**, 12734–12747.
34 X. Jing, H.-Y. Mi, B. N. Napiwocki, X.-F. Peng and L.-S. Turng, *Carbon*, 2017, **125**, 557–570.
35 G. Wu, M. Panahi-Sarmad, X. Xiao, F. Ding, K. Dong and X. Hou, *Composites, Part A*, 2021, **145**, 106373.
36 B. K. Ahn, D. W. Lee, J. N. Israelachvili and J. H. Waite, *Nat. Mater.*, 2014, **13**, 867–872.
37 K. Yang, X. Yin, Y. Yan, G. Luo, M. Xu, P. Pi, S. Xu and X. Wen, *J. Appl. Polym. Sci.*, 2020, **137**, 49309.
38 A. K. Gill, S. Riyajuddin, M. Alam, K. Ghosh and D. Patra, *Eur. Polym. J.*, 2020, **124**, 109455.
39 E. J. Son, J. H. Kim, K. Kim and C. B. Park, *J. Mater. Chem. A*, 2016, **4**, 11179–11202.
40 Y. Peng, M. Pi, X. Zhang, B. Yan, Y. Li, L. Shi and R. Ran, *Polymer*, 2020, **196**, 122469.
41 X. Zhang, B. C. Shiu, T.-T. Li, X. Liu, H.-T. Ren, Y. Wang, C.-W. Lou and J.-H. Lin, *Chem. Eng. J.*, 2021, **426**, 131923.
42 B. Li, D. Ni, J. Fan and J. Zhou, *Chem. Eng. J.*, 2022, **445**, 136818.
43 L. Huang, X. Yang, L. Deng, D. Ying, A. Lu, L. Zhang, A. Yu and B. Duan, *ACS Appl. Mater. Interfaces*, 2021, **13**, 16106–16117.
44 S. R. Ha, S. Park, J. T. Oh, D. H. Kim, S. Cho, S. Y. Bae, D. W. Kang, J. M. Kim and H. Choi, *Nanoscale*, 2018, **10**, 13187–13193.
45 W. Liang, L. Xu, S. Sun, L. Lan, X. Qiu, R. Chen and Y. Li, *ACS Sustainable Chem. Eng.*, 2016, **5**, 460–468.
46 J. Huang, W. Zhang, H. Li, X. Yu, S. Ding and C. Wu, *J. Mater. Sci.*, 2020, **55**, 17255–17265.
47 R. Salgado, R. del Rio, M. A. del Valle and F. Armijo, *J. Electroanal. Chem.*, 2013, **704**, 130–136.
48 Y. Wu, J. Liu, Z. Chen, Y. Chen, W. Chen, H. Li and H. Liu, *Polymers*, 2022, **14**, 5316.
49 X. Huang, Y. Wang, X. Wang, X. Yang, H. Zhang, F. Zhang, C. Wang, Y. Bai, Y. Liu, J. Wang, X. Wang, H. Chi, C. Zhou, K. Xu and P. Wang, *React. Funct. Polym.*, 2022, **179**, 105380.
50 G. Xue, Y. Shi, S. Wang, H. Zhou, Z. Chen, W. Guo, Y. Yang and M. Ye, *Chem. Eng. J.*, 2023, **456**, 140976.
51 X. Li, Z. Tan, B. Guo, C. Yu, M. Yao, L. Liang, X. Wu, Z. Zhao, F. Yao, H. Zhang, S. Lyu, C. Yuan and J. Li, *Chem. Eng. J.*, 2023, **463**, 142387.
52 A. Chae, G. Murali, S. Y. Lee, J. Gwak, S. J. Kim, Y. J. Jeong, H. Kang, S. Park, A. S. Lee, D. Y. Koh, I. In and S. J. Park, *Adv. Funct. Mater.*, 2023, **120**, 2213382.

